The Astrophysical Journal, 674:520–529, 2008 February 10

SOLAR MAGNETIC TRACKING. II. THE APPARENT UNIPOLAR ORIGIN OF QUIET-SUN FLUX

D. A. Lamb
Department of Astrophysical and Planetary Sciences, University of Colorado, Boulder, CO 80309-0391; dlamb@spd.aas.org

C. E. DeForest
Southwest Research Institute, 1050 Walnut Street, Suite 300, Boulder, CO 80302

H. J. Hagenaar
Lockheed Martin Advanced Technology Center, Org. ADBS., Building 252, Palo Alto, CA 94304

C. E. Parnell
School of Mathematics and Statistics, University of St. Andrews, St. Andrews, Scotland KY16 9S

and

B. T. Welsch
Space Sciences Laboratory, University of California at Berkeley, 7 Gauss Way, Berkeley, CA 94720-7450
Received 2007 February 23; accepted 2007 October 11

ABSTRACT

We investigate the origin of small-scale flux concentrations in the quiet Sun. In apparent violation of the physical requirement for flux balance, 94% of the features containing newly detected flux are unipolar at a resolution of 1.2″. We analyze 2619 of these apparent unipolar emergences in an image sequence from the *SOHO* MDI magnetograph and compare the ensemble average to a model of asymmetric bipolar emergence that could in principle hide opposing flux under the noise floor of MDI. We examine the statistical consequences of this mechanism and find that it cannot be responsible for more than a small fraction of the unipolar emergences. We conclude that the majority of the newly detected flux in the quiet Sun is instead due to the coalescence of previously existing but unresolved flux into concentrations that are large and strong enough to be detected. We estimate the rate of coalescence into arcsecond-scale magnetic features averaged over the solar surface to be 7×10^{21} Mx hr^{-1}, comparable to the reported flux injection rate due to ephemeral regions. This implies that most flux in the solar network has been processed by very small scale shredding, emergence, cancellation, and/or coalescence that is not resolved at 1.2″, and it suggests that currently unresolved emergences may be at least as important as ephemeral region emergences to the overall flux budget.

Subject headings: Sun: magnetic fields

Online material: mpeg animation

1. INTRODUCTION

Magnetochemistry describes the origin, evolution, and destruction of magnetic fields on the solar surface (Schrijver et al. 1997). In order to maintain the magnetic network, it is commonly thought (Simon et al. 2001; Krijger & Roudier 2003) that magnetic bipoles emerge into the solar photosphere in the interiors of supergranules. The poles of the bipole move apart and toward the supergranular boundary under the influence of the locally horizontal convective flow (Hart 1954; Leighton et al. 1962). Granular buffeting causes fragmentation and merging along the way and within the network. A given magnetic feature may fragment and merge many times before eventually canceling with one of the opposite polarity (including those from different parent bipoles). The addition of new bipoles and formation of new supergranules results in an evolving but statistically steady network (Simon et al. 2001).

Magnetic bipoles emerge on all observable scales (Harvey 1993). The largest, active regions, are associated with the solar cycle and are anchored at the base of the convection zone (Choudhuri 1992; Kosovichev et al. 1997), and they gradually dissipate under surface flows. Ephemeral regions emerge on the scale of supergranules (diameter ~ 15 Mm; Hagenaar et al. 1997) and appear to be the small end of the active region spectrum (Harvey 1993; Hagenaar 2001). Bipoles emerging on the scale of granules (diameter $\sim$ 1 Mm; Berger & Title 2001) appear to be more uniformly distributed over the surface, associated instead with a local dynamo. Flux has even been observed to emerge on scales as small as a few hundred km (De Pontieu 2002).

There is also a component of the photospheric magnetic field that is weak and horizontal and that occurs in places distinct from the network. These horizontal internetwork fields (HIFs; Lites et al. 1996) are typically small ($<1''$) and short-lived ($\sim$5 minutes), with weak polarization signatures and magnetic field strengths. De Pontieu (2002) observed longer lived but similar structures in longitudinal magnetograms taken at high viewing angles, such that a significant fraction of the horizontal field was directed along the line of sight. Among seven cases of flux emergence on small spatial scales ($<0.5''$), the two detailed examples he presented did not appear as bipoles, and only one (after some delay) showed weak signs of opposite-polarity flux. He interpreted this to be consistent with newly emerging flux seen at a high viewing angle.

We present observations of apparent unipolar magnetic flux generation observed in longitudinal magnetograms taken near disk center. These flux concentrations are nearly randomly distributed across the surface and are not associated with strong previously existing flux of either polarity. The geometry of the observations (the maximum angle between the vertical and the line of sight is 28°) prevents us from interpreting the data as HIFs, although we would not expect to see these, given the 1.2″ spatial resolution of the data.

We detect the unipolar flux emergences in a magnetogram sequence using an automatic feature-tracking algorithm. The algorithm identifies the method of birth and death for each feature, and those births that occur with no other features of either polarity nearby are called "unipolar Appearances," or just "Appearances," as described in the glossary of the first paper in this series (DeForest et al. 2007, hereafter Paper I). The leading capital letter indicates the event as one detected by our algorithm (which is necessarily limited by the cadence and resolution of the observations, among other things), rather than a physical event occurring on the Sun (as there should never be any true "appearances," since $\nabla \cdot \boldsymbol{B} = 0$), and we use this convention throughout.

Unipolar Appearances are the dominant source of flux injected on small but routinely detectable scales, and we interpret them as real manifestations of subresolution processes that prevent the detection of opposite-polarity flux. We have considered two models for unipolar Appearances: that they might consist of asymmetric newly emerged bipoles that preclude the detection of one pole, or that they might consist of previously existing flux that has coalesced either coherently or randomly due to the flow field of the surrounding granular convection cells. We have identified an observational technique (ensemble averaging) that can distinguish these two models and have applied it to a sequence of magnetograms from the MDI instrument aboard *SOHO* (Scherrer et al. 1995). We find that the great majority of Appearance events are not newly emerged bipoles with an asymmetric cross section. Instead, we infer that the events are due to the coalescence of undetected previously existing flux under the influence of converging surface flows.

In § 2, we briefly explain our data and the magnetic feature-tracking algorithm, which includes a step to classify the births of magnetic features. In § 3, we present the results of the birth classification and show that unipolar births are the dominant source of flux injection into the quiet Sun on scales above 1 Mm. We introduce an asymmetric emergence model in an unsuccessful attempt to explain the large numbers of unipolar Appearances as poorly detected bipolar emergence. We show that the coalescence of subresolution flux into arcsecond-scale concentrations can result in a perceived flux emergence rate that is comparable to that of larger ephemeral region bipoles. In § 4, we discuss possible interpretations of this "emergence rate" and its importance in sustaining the magnetic network.

2. OBSERVATIONS

2.1. *Magnetogram Preprocessing*

We use a nearly 24 hr sequence of 1 minute cadence MDI (Scherrer et al. 1995) high-resolution ($0.6''$ pixel^{-1}) magnetograms taken on 2005 October 13–14 near disk center. The raw magnetograms are despiked using the ZSPIKE algorithm in the SolarSoft software tree (Freeland & Handy 1998) to remove the effects of cosmic rays. The algorithm uses a pixel's second time derivative to determine if its value is too low or too high and replaces the bad value with the average of its two nearest temporal neighbors.

The despiked images are divided by a cosine factor to correct for the difference between the local vertical and the magnetograph line of sight at the solar surface. We acknowledge that the underlying assumption of a radial photospheric field may not be valid, given the weakness of the fields we consider (Harvey et al. 2007). Since MDI does not provide vector field information, this is the best that can be done. Regardless, the fact that the region under study is near disk center means that this is a small correction. We do not believe it to be likely that many of the unipolar Appearances discussed below are the result of an inclined field becoming radial at one end. In such a situation, with one pole of a bipole being radial and the other being severely inclined to escape detection by a longitudinal magnetograph, the total flux detectable by a longitudinal magnetograph is the same in both poles, provided that the observation is near disk center. This is because as the longitudinal field strength decreases due to inclination angle, the area of the pole increases by the same factor. The scenario presented below in Figure 4*a* is a variant of this scenario and should be detectable by the same method (ensemble averaging) used in this analysis, provided that a filter-based magnetograph's line-of-sight Zeeman sensitivity is independent of the field geometry, as is usually assumed.

The magnetograms are then derotated (DeForest 2004) to remove proper motion due to solar rotation; the derotation also compensates for foreshortening effects. Finally, the magnetograms are temporally averaged using a 10 minute FWHM Gaussian weighting with a 5 minute cadence and then are spatially smoothed with a 3 pixel FWHM Gaussian kernel. The spatial smoothing reduces granulation noise, and the temporal smoothing reduces the noise from photon counting statistics and from the solar p-modes at the expense of increasing the evolution blur. Since the temporal averaging kernel is wider than the cadence between frames, there is some cross-talk between the averaged frames, such that we oversample the data on the time axis. However, we consider that an acceptable consequence for achieving low noise in this data set. To measure the noise in the processed magnetograms, we assume that the cores of the histogram of magnetogram values are Gaussian and due to noise. We fit a parabola to the cores of the magnetogram histograms in logarithmic space, as done by Hagenaar et al. (1999), and derive an average noise level of $\sigma = 1.93 \pm 0.03$ G. At the completion of image preprocessing, our data set is 284 frames at a 5 minute cadence of 673×980 pixel, $0.6''$ pixel^{-1} radial magnetograms. The raw magnetograms are 1024×1024 pixels, but in the process of derotation we crop the frame so that no portion of the tracked region passes into or out of the MDI high-resolution field of view. An example magnetogram with the identified and tracked features outlined is shown in Figure 1.

2.2. *Event Classification*

Feature-tracking methods have been detailed in Paper I. For this analysis we use the SWAMIS software described in that paper and focus on the final step, event classification, in which we determine the method of birth and death for each feature in the data set. To determine the birth method of each feature, we examine a region around the birth location in the birth frame and the frames immediately before and after. We define and describe the following birth events and show an example of the four major types in Figure 2:

Appearance.—There are no other features in the vicinity.

Emergence.—A feature is born near another of opposite polarity, and flux is approximately conserved.

Fragmentation.—A feature is born near another of like polarity, and flux is approximately conserved; or, there is sufficient overlap between a new feature and a like-polarity feature in the previous frame.

Complex.—A birth satisfies the proximity and flux conservation requirements of an Emergence with one feature and a Fragmentation with another; the number of these events is typically small.

Error.—A birth satisfies the proximity and polarity requirements of an Emergence or Fragmentation but does not approximately conserve flux; the number of these events can be significant.

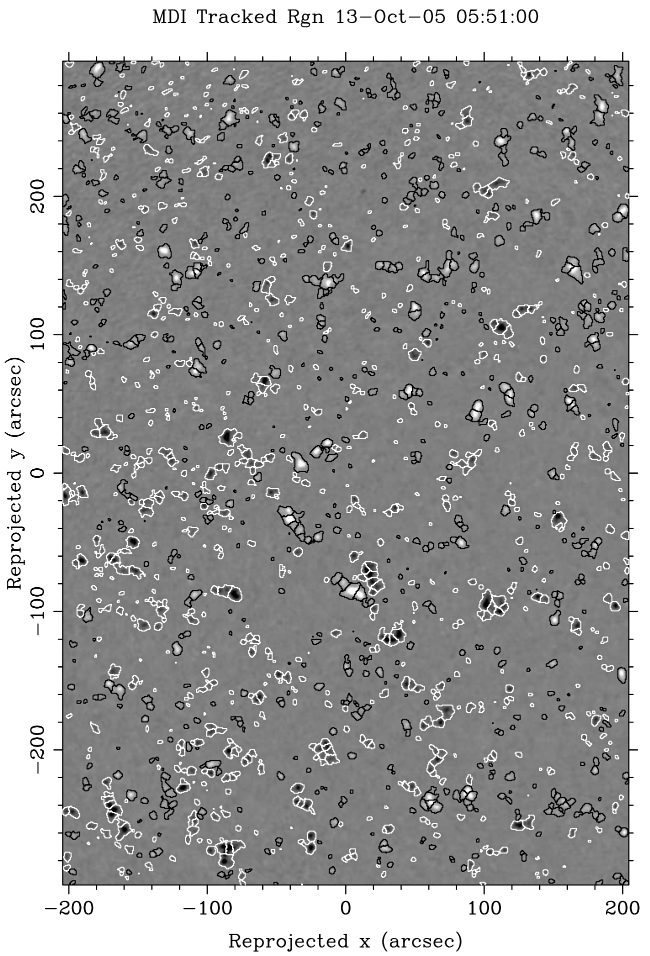

Fig. 1.—Example magnetogram frame with the identified concentrations outlined in black (positive) and white (negative). The magnetic flux density saturates at ±100 G. [*A color movie showing the tracking of the entire data set is available in the electronic edition of the Journal.*]

The death events Disappearance, Cancellation, and Merger are defined as the birth events Appearance, Emergence, and Fragmentation, respectively, run backward in time. Since a Fragmentation, Emergence, Merger, or Cancellation is necessarily a two-body interaction, we also record the identity of this other feature (dubbed, in analogy to grammar, the object of the interaction).

There are two important parameters adjustable by the user that influence the number of each type of event. If t is the birth frame, b is the feature that was born, and i is the object, then the ratio r of their changes in flux ϕ is

$$r = \min\left\{\frac{\phi_{t-1}^{i} - \phi_{t+1}^{i}}{\phi_{t+1}^{b}}, \frac{\phi_{t+1}^{b}}{\phi_{t-1}^{i} - \phi_{t+1}^{i}}\right\}. \qquad (1)$$

To satisfy approximate flux conservation, $r \geq R$, where R is the first parameter determined by the user. The quantity R is the factor within which the change in fluxes must agree for the event to be classified as flux-conserving. Typically we use a value of $R = 0.5$; higher values, which require stricter flux conservation, result in many Error events. Note that Hagenaar (2001) used a value of $R = 0.33$ in a single image to identify features that were ephemeral region bipoles. Lowering R reduces the number of Errors and increases the number of Emergences, Fragmentations, and Complexes, but we note that setting $R = 0$ (only requiring the sign of the flux changes to be correct, neglecting their magnitudes) still produces some Errors. This approximate flux conservation is required because of fundamental limitations in detecting all of the flux in each feature. Because of noise constraints, we consider a pixel to be part of a feature only if it satisfies two requirements: (1) it has an average flux density greater than 8 G, and (2) one of its neighboring pixels, or one of its neighbor's neighbors (ad infinitum in both space and time), must have an average flux density greater than 10.6 G. These thresholds correspond to roughly 4 and 5 σ; see Paper I for a detailed description of this dual threshold hysteresis detection method. If a flux concentration has an extended component with a flux density of less than 8 G, our algorithm will not detect a considerable amount of the total flux in the concentration. Higher resolution observations with an increased sensitivity to weak fields would ameliorate the situation, but, lacking those observations, we can only perform longer averaging to beat down inherent noise in the magnetograms, reducing spatial and/or temporal resolution at the risk of missing some essential physics.

The second parameter is the maximum distance by which interacting features may be separated. Smaller values increase the number of features found alone (Appearances). We typically use a separation distance of 5 pixels to determine whether two features may be interacting.

3. ANALYSIS

We use the data and code described above, with detection thresholds of 8 and 10.6 G, the "downhill" method of feature identification, and filter criteria (lifetime of $\geq$3 frames, maximum size of $\geq$4 pixels, and volume of $\geq$12 pixels). For event classification we use $R = 0.5$ and a maximum separation of 5 pixels. We track 31,799 individual features in the 284 frame data set. We noted in a movie of the tracked magnetogram sequence (included in the electronic edition of the *Journal*) that the northern portion of the field of view, above approximately $y = 100''$ in reprojected coordinates (Fig. 1), was much more noisy than the rest of the field of view. This is likely due to variation of the central wavelength of the MDI interferometers across their faces (cf. Scherrer et al. [1995], especially Fig. 9 and accompanying text). Therefore we eliminate features that are born and die above this coordinate, further reducing the size of the analyzed region to 673×654 pixels. We also eliminate features that were present at the beginning of the data set. There are 15,595 remaining features, providing an average unsigned network density of 1.8 ± 0.4 Mx cm^{-2}.

Somewhat alarming at first is the large number of Error events—events for which no possible Emergence or Fragmentation conserved flux. These Errors represent 21% of the births in the data set. A given Error event may have more than one object as long as none of the interactions conserve flux, and on average there are 1.4 interactions per Error event. We find that, of all the possible feature interactions that led to an Error classification, 61% are interactions of like-polarity features. This indicates that 61% of the Error events might be physical fragmentations that failed (due to instrumental or algorithmic limitations) to conserve flux.

Similarly, 39% of the Error events might be bipolar emergences that simply failed to conserve flux. If this were the case, then these opposite-polarity Errors may be responsible for over 5 times the flux introduced by bipolar Emergences that did conserve flux, potentially reducing the photospheric recycling time ($\sim$14 hr; Hagenaar 2001) by a factor of 6. For simplicity, we have analyzed the 425 Error events for which there is only one object and the object is a feature of opposite polarity. We find that more than half of the objects were born over 100 minutes *before* the Error event and that only 15% are born within 15 minutes of the Error event. In addition, more than half of the objects have more

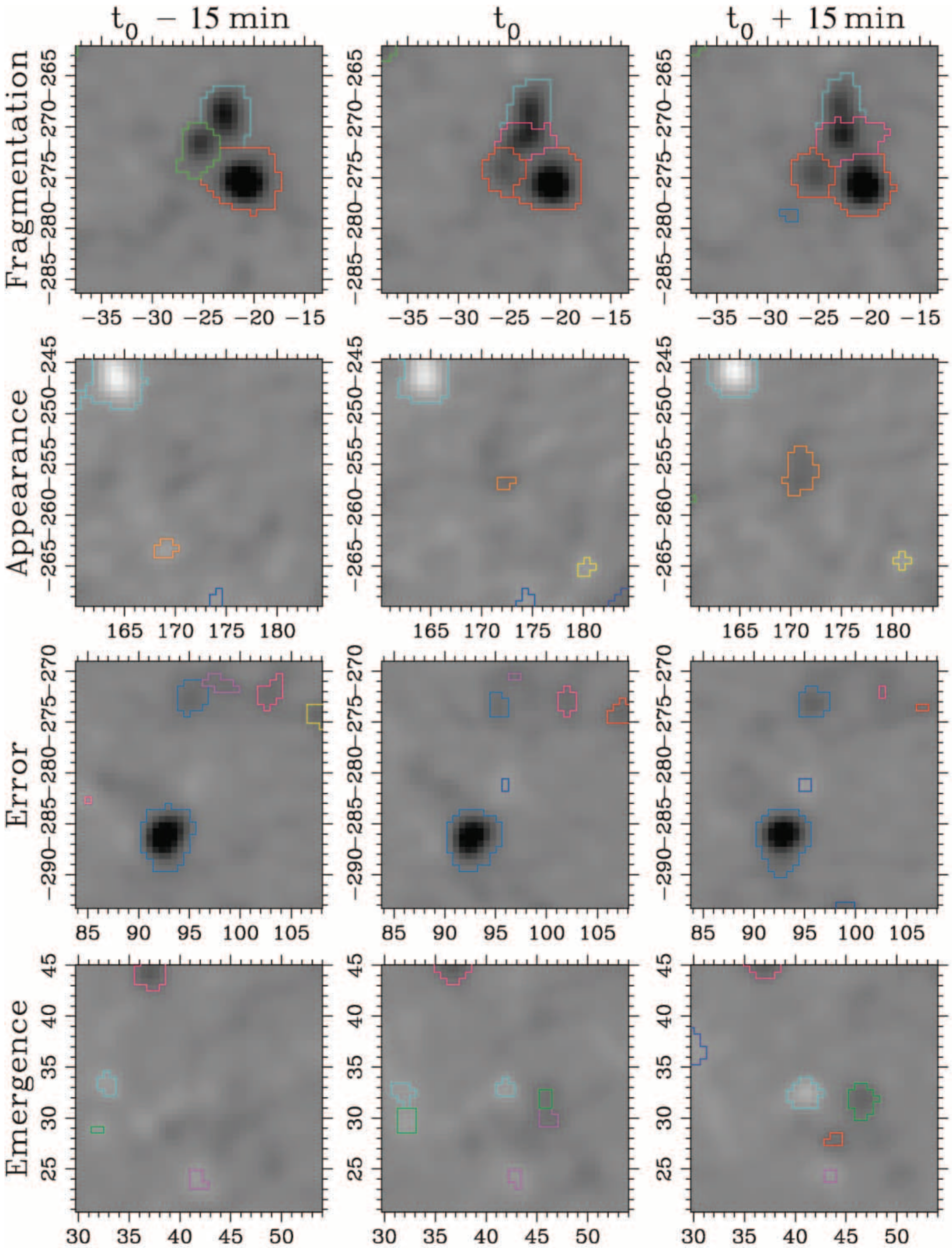

Fig. 2.—Example showing each of the four main birth event types. The left panels show the magnetogram before the birth, the middle panels show the magnetogram at the moment of the birth, and the right panels show the magnetogram after the birth. The feature born by the given event type is at the center of each frame in the middle column. The *x*- and *y*-coordinates are scientific coordinates and match the coordinate system of the movie accompanying Fig. 1. All features shown here were born on 2005 October 13, and the birth times from top to bottom are 21:41, 23:16, 10:26, and 10:21. In all panels we have saturated the magnetogram at ±50 G in order to increase the visibility of the weak field.

than 15 times the flux of the new feature at the time that it was born. We suggest that Errors with opposite-polarity interactions are not bipolar emergences that failed to conserve flux, but we defer further discussion until § 4.

Figure 3 shows the positions of Fragmentations, Appearances, and Errors in relation to each other and the existing magnetic field. There is no obvious correlation between Error events and either Fragmentations or Appearances. The only obvious correlation observed is that Errors tend not to occur near strong features [such as the V-shaped bipole around (10, −80)], but rather occur in regions of weak field [such as that around (10, 0)]. This suggests that many of these Errors are due to processes that are below the resolution and sensitivity of the instrument and our tracking algorithm. However, since they are not well separated from other flux when they are born, they are not directly relevant to analysis of Appearances with no features nearby.

Since we are interested in the formation of the magnetic network, it is useful to calculate the amount of flux injected by each

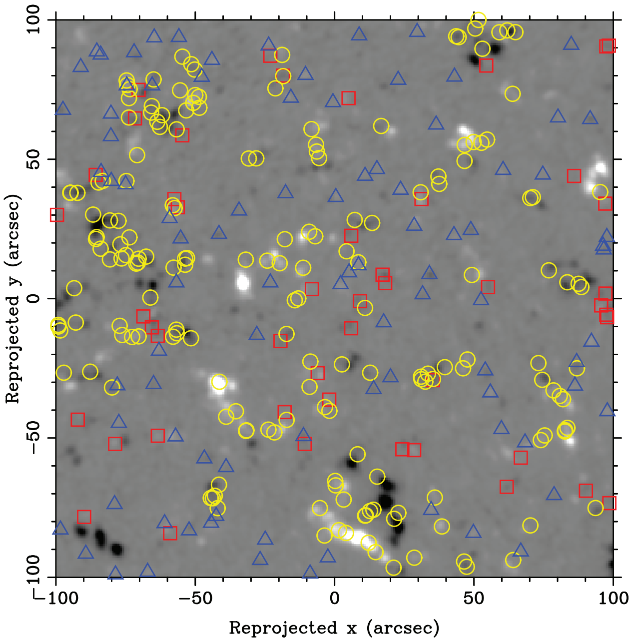

FIG. 3.—Birth locations of new features in a subset of the field of view, relative to other births and the existing field. The background magnetogram corresponds to that of 2005 October 13 08:21 UT, and the birth events shown are those that occur between 07:21 and 09:21 UT. Red squares correspond to Errors, yellow circles to Fragmentations, and blue triangles to Appearances. There is no obvious correlation between the Errors and the other birth events, but we note that Errors tend to occur in areas of weaker field strength.

type of event. While Fragmentations are numerous, we note that they merely rearrange flux, and we must look to the other birth mechanisms for the injection of new flux. By looking only two frames (10 minutes) after the birth of each feature, we are able to calculate the flux from all 15,595 features in the data set. But since this is a short time compared to the recycling time of the network (Hagenaar 2001), we also calculate the flux from those 6356 features that survived for at least 12 frames (60 minutes). The percentage of birth events and of flux introduced by each event type is shown in Table 1. Since only Emergences and Appearances inject new observable flux into the photosphere, it is important to compare the amount of new flux injected by these events. Appearance is the birth method for 30% of all features, but when Fragmentations and Errors are excluded, Appearances account for 94% of all births that inject new flux into the photosphere. In comparison, the number of births due to Emergence is small. Unipolar Appearances exceed bipolar Emergences by factors of 18 in number and 14 in flux. For those features that are still alive after 60 minutes, the ratios between the Appearances and Emergences are about the same: features born by Appearance exceed features born by bipolar Emergence by factors of 20 in number and 12 in flux. Features born by Appearance are not more short-lived than those born by other methods, and so they cannot be ignored.

The removal of magnetic flux from the photosphere is just as important as the injection of flux. When all features are considered, the distribution of death types is similar to the distribution of birth types given in Table 1. However, slightly more than 50% of features born by Appearance die by Disappearance (compared to the roughly 20% of all features that die by Disappearance). We do not believe that these features are inherently different from features that are born by Appearance and die by other means. For example, the lifetime distributions of the two categories are essentially the same. As with the Appearances, we interpret the Disappearances as flux dispersal (time-reversed coalescence), and we will study this in more detail in a future paper in this series.

3.1. *Asymmetric Emergences*

The presence of large numbers of Appearances and small numbers of bipolar Emergences is not unique to this data set or feature-tracking algorithm (Paper I) and therefore warrants further investigation. The simplest explanation of unipolar Appearances is bipolar emergences with an asymmetry that renders one pole less detectable. For example, in Figure 4*a*, one pole has a larger area than the other. Since the flux in the two poles must be equal, the larger pole has a weaker average field strength and so does not rise above our detection threshold.

In this picture, an apparent unipolar Appearance could occur because one pole is detectable and the other is not. While we cannot alter the instrument collecting the data, we can produce an ensemble average of many such events to remove the noise and lower the effective detection threshold. Co-aligning and averaging many such events (while homogenizing the sign of the feature) yields an arbitrarily low detection threshold, such that the ensemble average of many such asymmetric emergence events should yield a "sombrero" distribution, as shown in Figure 5*a*. The radius of the "brim" is determined by the typical separation speed and the elapsed time before detection. If asymmetric emergence is the main mechanism by which fresh unipolar Appearances occur, then the peak and brim of the sombrero should have equal and opposite volumes. This equality is robust against variations in the separation distance and relative strength of emergence events, because total signed flux is conserved in the averaging process, while incoherent noise is mostly averaged out.

We have developed an asymmetric emergence model with which to compare our observations. In each of several initially blank image fields, we randomly place a positive two-dimensional truncated ($\pm 3\sigma_P$) flux concentration with a Gaussian profile. The

TABLE 1
PERCENTAGE OF EVENTS AND FLUX BY BIRTH EVENT

Event	After 10 Minutes ($N = 15{,}595$) Events (%)	After 10 Minutes Flux (%)	After 60 Minutes ($N = 6356$) Events (%)	After 60 Minutes Flux (%)
Fragmentation	47.9	82.3	45.6	76.0
Error	20.6	8.6	17.6	10.9
Appearance	29.6	8.4	35.0	12.0
Emergence	1.6	0.6	1.7	1.0
Complex	0.2	0.1	0.2	0.1

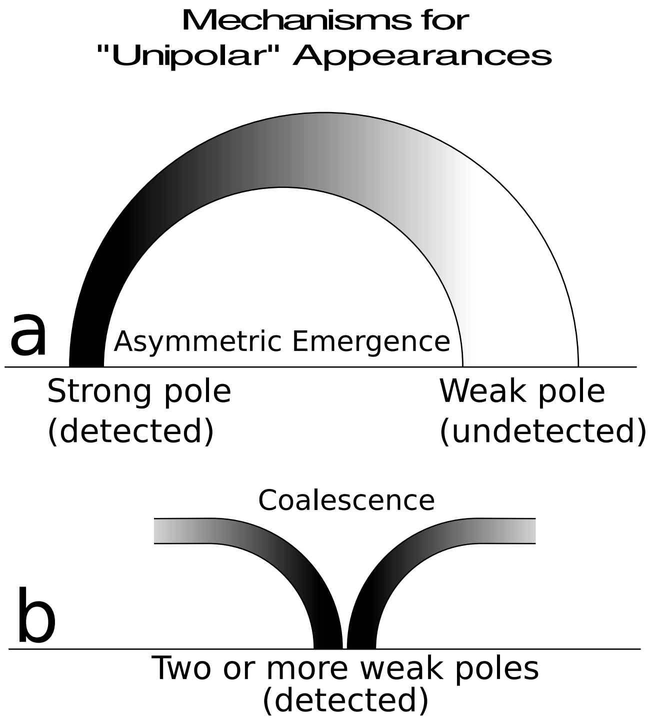

FIG. 4.—Two scenarios for detecting negative (*black*) flux while hiding the positive (*white*) component. (*a*) The cross section of the positive end of the flux tube is larger, so the weaker average field does not exceed the tracking detection threshold. (*b*) Each end of the flux tube is not detectable by itself, but if two or more like-polarity ends come together, the average field strength can exceed detection limitations for that polarity only. In this case the tubes are not newly emerging, so the positive ends could be arbitrarily far away at the time of detection.

positive concentrations have peak strengths and standard deviations that are chosen randomly, but within a range that matches observations ($B_{\max} \sim 8$ G; $\sigma_P \sim 1$ Mm). Near each positive concentration, we place a two-dimensional truncated ($\pm 3\sigma_N$) negative concentration with a Gaussian profile. In a given model run, the peak strength of the negative concentration is smaller than that of the positive concentration by a factor that we determine. In this paper, we use factors of 2 and 10. The factor-of-2 asymmetry is a lower bound beneath which the asymmetry of the cross sections would be too small and the larger pole would be detected by our algorithm. The factor-of-10 asymmetry is a reasonable upper bound estimated from convection simulations (e.g., Fig. 5 of Cattaneo et al. 2003). Since the total unsigned flux in each concentration of the pair is equal, the negative concentration will have either twice or 10 times the area of the positive concentration ($\sigma_N^2 = 2\sigma_P^2$ or $\sigma_N^2 = 10\sigma_P^2$), depending on which case is used. The separation of the concentration centers is $5\sigma_P$, proportional to the width of the positive concentration, which is geometrically plausible. This separation gives minimal interference between the two halves of the model distribution, without applying excessive separation. We avoid applying excessive separation of the model poles because a freshly emerging bipole should be compact. With sufficient time resolution, the two poles of a newly emerged bipole will be adjacent by virtue of their geometric connection.

We use the noise value derived from the processed data, $\sigma = 1.93$ G, and add it to the synthetic asymmetric emergence magnetogram. The noise added to the synthetic magnetogram is not a completely accurate emulation of the real magnetogram noise, which has sources other than shot noise (for example, evolution noise may cause the noise value in one pixel to be correlated with the noise value in a neighboring pixel), but it is sufficient for our current purposes.

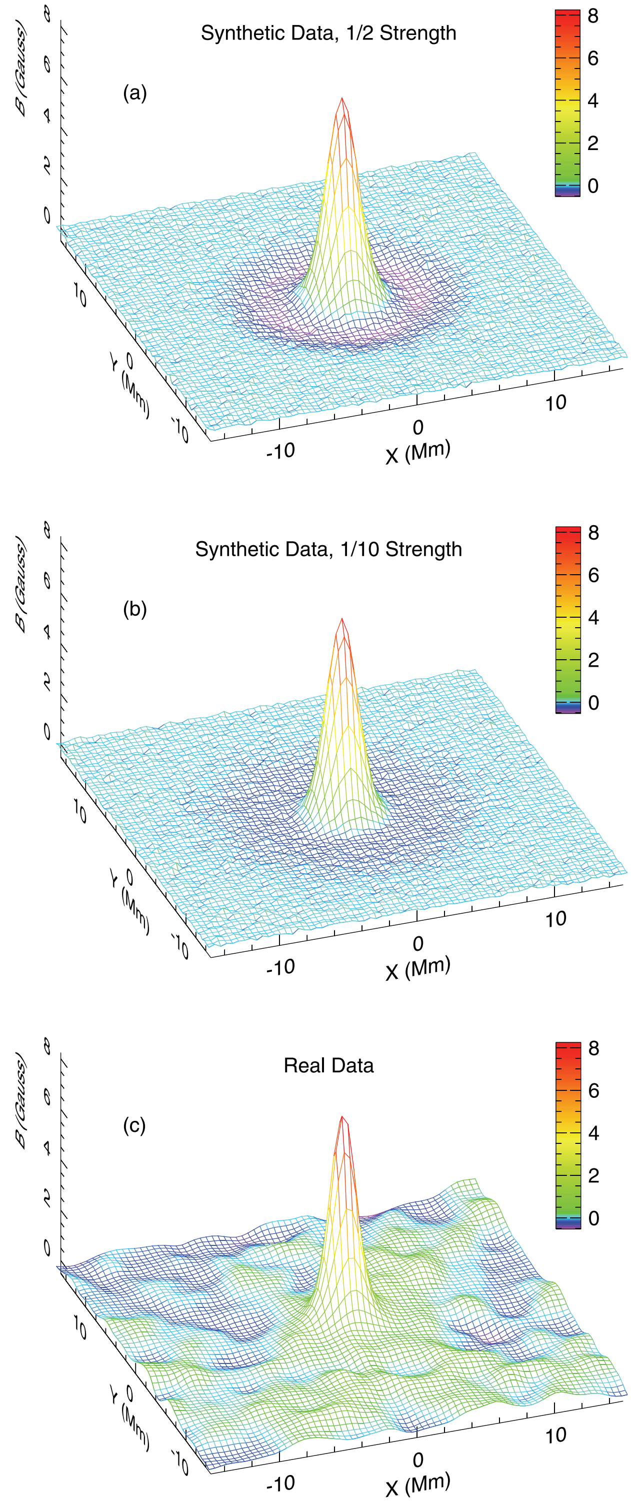

FIG. 5.—(*a*) Surface plot of a composite of 2619 synthetic asymmetric emergences in which the negative pole is half the strength of the positive pole. A negative trough (*blue and purple*) is visible around the peak. (*b*) Surface plot of 2619 synthetic asymmetric emergences in which the negative pole is 1/10th the strength of the positive pole. A very faint blue negative trough is visible, even with this large asymmetry. (*c*) Surface plot of a composite of 2619 detected Appearances with initial sizes between 1 and 4 pixels. Here a small trough is visible, indicating that some events may be due to bipolar emergence, but it is not negative, which indicates that the vast majority of events do not have an opposing feature nearby.

To demonstrate the appearance of a data set with asymmetric emergence, we generated two artificial data sets with 2619 randomly generated model asymmetric emergence events (one for each small Appearance found in our data). One of the data sets is the half-strength case, the other is the 1/10th-strength case. In all cases, the total flux in the poles of each bipole is the same, but the field strength varies. We compared these model data sets with real data by subjecting all data sets to the same ensemble averaging process: we co-aligned fresh Appearance events and produced an ensemble average. Plots of the "sombrero distributions" are shown in Figure 5. There is an obvious trough in the half-strength synthetic data, colored blue and purple. The trough in the 1/10th-strength synthetic data is not as clearly apparent, but can be seen as a wide blue ring around the base of the central peak. There is no visible trough in the real data; the lowest values in the real data are also colored blue and are far away from the central peak.

The real data in Figure 5*c* are the ensemble average of those 2619 Appearances that have an initial size of less than 5 pixels (<1 Mm^2). The size constraint is intended to guard against the possibility of a small concentration hiding in a large opposite-polarity concentration. We do not include in our averaging process the 438 small Appearances that originated close to the edge of the field of view.

In order to provide quantitative results and further reduce background noise, we averaged over azimuth. We converted each (x, y) composite image into an (r, θ) plot by unwrapping the image about the central peak and then summing over θ. Here it is important that the unwrapping is done correctly so that the total flux in an annulus is preserved, not the flux density in each pixel. Otherwise a large flux from a small number of pixels near the peak of the (x, y) image will have a disproportionately large effect on the (r, θ) image. For a two-dimensional Gaussian-shaped flux concentration,

$$B(r) = B_{\max} \exp\left(-\frac{r^2}{2\sigma^2}\right), \quad (2)$$

the total differential flux $d\Phi$ in the thin annulus between $r' - dr'/2$ and $r' + dr'/2$ is

$$d\Phi(r') = 2\pi\sigma^2 B_{\max} \times \left\{ \exp\left[-\frac{(r' - dr'/2)^2}{2\sigma^2}\right] - \exp\left[-\frac{(r' + dr'/2)^2}{2\sigma^2}\right] \right\}, \quad (3)$$

and, for $r' \ll \sigma$,

$$d\Phi(r') \approx 2\pi B_{\max} r'\, dr'. \quad (4)$$

Thus, the flux in an annulus increases linearly at short distances, instead of decreasing as the two-dimensional flux concentration does. Figure 6 shows a plot of flux per unit radius in a thin annulus $[d\Phi(r')/dr']$ versus distance from the central peak for the synthetic and real data in Figure 5.

Figure 6*c* shows no evidence of the trough shown in Figures 6*a* and 6*b*, but this was also surmised from the surface plots in Figure 5. However, converting from a surface plot to the profiles in Figure 6 makes the detection of the trough much easier, as seen in the 1/10th-strength case. In addition, we are able to measure the areas of the peak and trough in the synthetic case, and we find that they are equal to within a few percent, as expected. Had there been a trough in the real data, the ratio of peak to trough areas

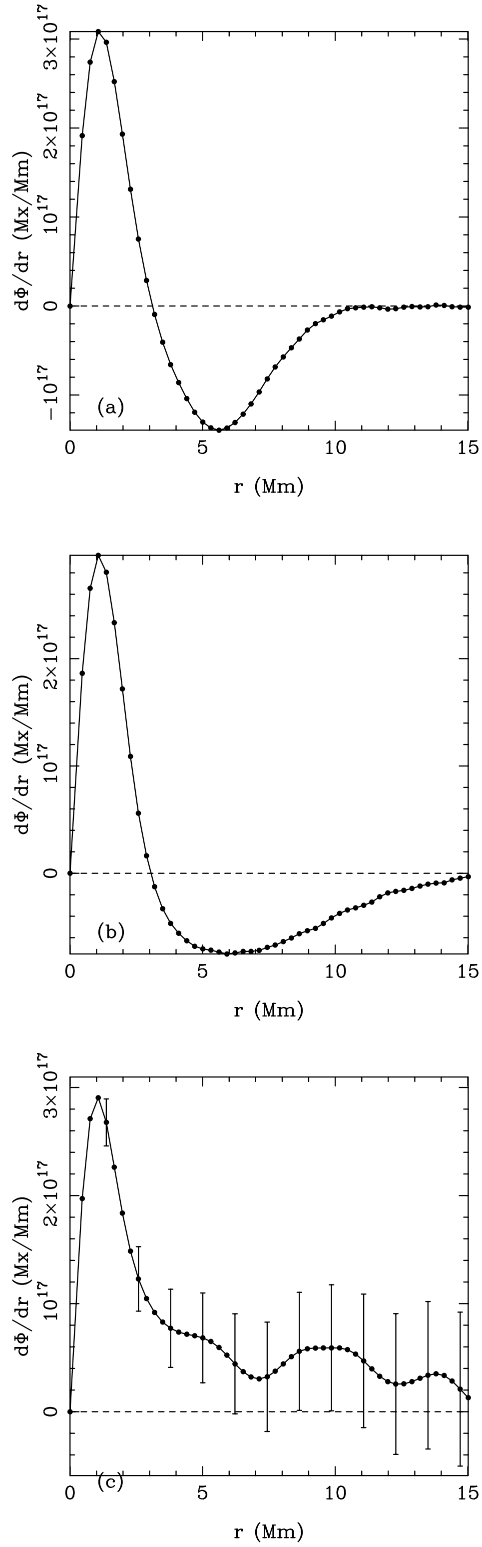

Fig. 6.—Flux per unit radius, as a function of distance from the center of the peak of the synthetic data in Fig. 5. The value at each point is the total flux in an annulus centered on the distribution peak, corrected for the width of the annulus. For the synthetic cases, the areas of the peak and trough are equal to within 1.0%. The data are oversampled by a factor of approximately $\sqrt{2}$ due to the interpolation done when converting the composite magnetogram to an (r, θ) plot. The 1 σ error bars in the real data are shown only on every fourth point for clarity. They are calculated a priori on the basis of our sampling method and a coherent noise source (granules with diameter of 1 Mm). These error bars are not shown for the synthetic data, since the Gaussian noise that we added is incoherent.

would have indicated the relative importance of the coalescence and asymmetric emergence models.

Our failure to detect a trough in the real data is not due to an uncorrected offset in the average background field. For a uniform field, the total flux per unit radius in an annulus increases linearly with distance and would intersect the y-axis at the origin, and no evidence of such a field exists in Figure 6*c*. The increases around 10 and 14 Mm are due to small fluctuations in the composite background field. If an Appearance forms in the interior of a supergranule, as is suggested by Figure 3, then at distances of 7–15 Mm from the Appearance we expect to find the supergranular network, which consists of structured, coherent noise that would not disappear after averaging. The fact that these fluctuations do not average out implies that the flux in Appearing features is biased toward having the same sign as the nearby network concentration, which is consistent with it shredding off that concentration.

To check the possibility that we have not averaged over a large enough area around each peak, we increased the area by factors of 2 and 8, and no evidence for a trough was seen in these tests. Figure 7 shows a plot of flux per unit radius as in Figure 6*c*, but with an averaging window that extends 43 Mm from the Appearance. Beyond the increase that peaks around 10 Mm (also present in Fig. 6*c*), there are several other peaks and troughs, including a large peak at a distance of approximately 40 Mm. In spite of these local minima and maxima, there is no distance at which the flux per unit radius is negative. The error bars are large compared to the photon noise error bars because the surviving noise is nearly all due to leak-through of granulation, with fewer spatial and temporal samples than pixels.

Our null measurement that no trough is present is a strong one that is not directly affected by MDI's point-spread function. Should the point-spread function expand the central peak to apparently cancel some of the subthreshold opposing pole, an equal amount of the peak flux would also be eliminated from detection, preserving the peak/trough balance of the resulting sombrero plot.

3.2. *Flux Coalescence Rate*

After initially becoming visible on the solar surface, magnetic features fragment and merge with other features multiple times before canceling and (presumably) submerging. From the current work, it is apparent that, at least at the 1 Mm scale, the coalescence of previously unobservable flux into concentrations strong and large enough to be observed is more important than bipolar emergence for introducing observable magnetic features into the photosphere. Similarly, observed flux may disperse instead of canceling, and a given elemental flux tube may coalesce and disperse many times before finally canceling. Here we provide a first estimate of the flux coalescence rate.

Hagenaar et al. (2003) measured the total flux introduced by ephemeral regions in MDI full-disk magnetograms. Since the flux in an ephemeral region naturally evolves over time, the most sensible way to calculate the total flux introduced by ephemeral regions was to calculate the maximum flux in each ephemeral region and sum them. We perform the same calculation here: for every feature born by Appearance, we find the maximum unsigned flux and then add these together. We scale this result by assuming that the process is homogeneous over the solar surface, in order to compare with other published flux emergence rates. We find that 7×10^{21} Mx hr^{-1} coalesces above the 8 G detection threshold. Similarly, the flux dispersal rate is calculated by summing the maximum unsigned fluxes of all features that died by Dispersal, and we find a rate of 5×10^{21} Mx hr^{-1}. These rates are comparable to the rate of flux emergence due to ephemeral regions that was quoted by Schrijver et al. (1997), which was 3×10^{21} Mx hr^{-1}.

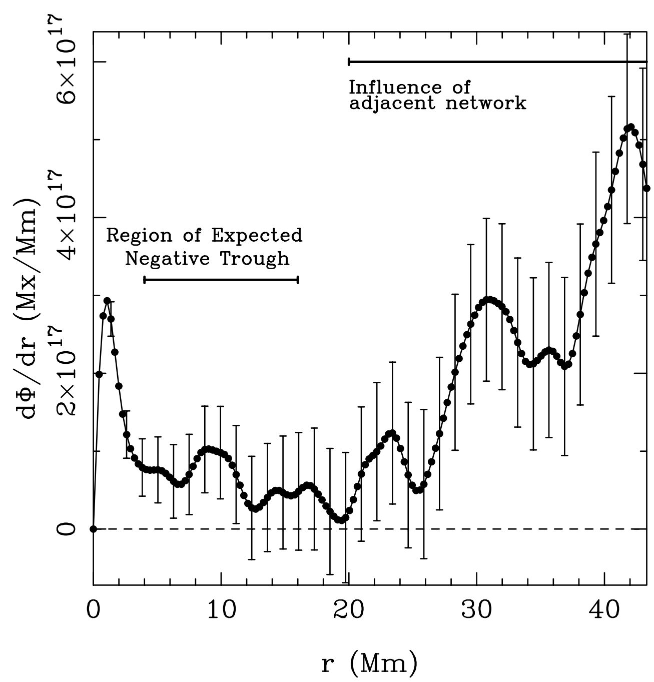

Fig. 7.—Flux per unit radius as a function of distance, for the real data. Similar to Fig. 6*c*, but extended to 43 Mm. Because of the larger averaging area, more events are found near the edge of the tracked field of view, and so we only average over 1806 events instead of 2619. The increase seen in Fig. 6*c*, which peaks near 10 Mm, is also visible here, and additional increases and decreases in the flux are seen at larger distances.

4. DISCUSSION AND CONCLUSIONS

We have performed feature tracking on a nearly 24 hr sequence of MDI high-resolution ($0.6''$ pixel^{-1}) magnetograms. In the 673×654 pixel (44 arcmin^2) region considered, we have identified 15,595 new and unique magnetic features. By identifying the method of birth of each feature, we find that features born by Appearance (with no other feature within 5 pixels) are responsible for over 10 times the amount of photospheric flux as features born by bipolar Emergence.

A significant fraction (20%) of our detected birth events do not conserve flux to within a factor of 2, and we have calculated that 40% of these non–flux-conserving events are likely due to opposite-polarity interactions. This indicates that we may have failed, for either instrumental or algorithmic reasons (or both), to properly detect the opposite pole. However, we find that in only 15% of these opposite-polarity interactions was the opposing feature born within 15 minutes of the new feature, and we take this as the fraction of Error events that are likely bipolar emergences that we failed to detect. The flux introduced by these failed emergences may be of the same order as the flux introduced by the successful emergences ($8.6\% \times 40\% \times 15\% = 0.5\%$, compared with 0.6% for Emergences in Table 1). Even granting this possibility only doubles the flux introduced that is due to Emergences, and this does not greatly affect the relative importance of the Appearance events.

Over 4600 of these Appearances are found in the data set, and 2619 of them (those with small initial sizes) are used to understand the apparent "unipolar emergences" seen by many feature-tracking codes (as described in Paper I). We tested a straightforward model in which features detected as Appearances are the stronger pole of a small, asymmetrically emerging bipole, and we compare the ensemble average of these "asymmetric emergences" with the ensemble average of the 2619 small Appearances. If such a situation were the dominant cause of Appearances, the ensemble average would resemble a sombrero, as in Figure 5*a*, with the central peak caused by the feature detected as an Appearance and the trough caused by the opposite-polarity feature that escaped detection. We find no hint of a trough in the ensemble average of the Appearances, and so we conclude that "asymmetric emergence" cannot be responsible for more than a small fraction of Appearance events, on the basis of analysis of MDI data.

Rather, we conclude that at the time of origin of most new magnetic features in the quiet Sun, there is no associated opposing pole nearby. This implies that most newly Appeared magnetic features are caused by processes that are not directly detectable by MDI. In particular, these events must be caused by the coalescence of existing flux into concentrations that are large enough to be detected. The existing flux may be coherent (as a large, weakly magnetized area that is concentrated, for example, by supergranular flows) or may result from a large number of currently unresolved bipolar emergences that happen to accumulate one polarity at a particular zone of convergence (e.g., DeForest & Lamb 2004). An example of the latter can be seen in Figure 7 of Hagenaar & Shine (2005), which compares an MDI high-resolution magnetogram ($0.6''$ pixel^{-1}) of a sunspot to a cotemporal and cospatial Swedish Vacuum Solar Telescope (SVST) magnetogram ($0.05''$ pixel^{-1}). In this comparison, several features appear to be unipolar in the MDI magnetogram but are found to each consist of multiple features of both polarities in the SVST magnetogram. These and other recent observations show new kinds of magnetic structure at high resolution (Berger et al. 2004), giving credence to the idea that our observed unipolar Appearances are due to the coalescence of small previously existing magnetic fields, rather than to fresh emergences.

The idea of flux coalescence is not new (Martin 1988), but it has not been measured before. We estimate that the random aggregation of flux below the MDI resolution limit that results in features detectable by MDI is, within the measurement uncertainties, as important for injecting flux into the photosphere as ephemeral regions (7×10^{21} Mx hr^{-1} for coalescence and 3×10^{21} Mx hr^{-1} for ephemeral regions, over the entire solar surface). Even if we consider only the roughly 50% of features that are born by Appearance but do not die by Disappearance, it seems possible that the network is primarily sustained not by the emergence and breakup of ephemeral regions and other relatively large concentrations (Simon et al. 2001), but rather by the aggregation of many smaller (subarcsecond) magnetic features. A combination of the two processes is nearly certain (e.g., Schrijver et al. 1997), but the current result indicates that the latter is the predominant source of new features.

We find a flux dispersal (time-reversed coalescence) rate of 5×10^{21} Mx hr^{-1}, which is comparable to the coalescence rate. Approximately half of the features that are born by Appearance (inferred coalescence) die by Disappearance (inferred dispersal); however, these features do not seem to be inherently different from features that are born by Appearance and die by other means. For example, if the Appearing/Disappearing features were merely statistical fluctuations that were due to noise, one would expect their average lifetime to be much shorter than those of Appearing/Canceling features, since the latter would take longer to find an opposite-polarity feature with which to cancel than would be expected from a chance fluctuation of the measured background field. We do not find such a difference. The coalescence and subsequent dispersal of flux at roughly the same location may provide some insight into the physical mechanism by which this occurs, but we defer a full analysis on the removal of flux from the photosphere to a future paper in this series.

Our coalescence rates imply unresolved motion and processing of flux, which is likely to include a strong emergence component. This suggests that observed emergence events are but the tip of a statistical iceberg, whose unseen component consists of huge numbers of tiny emergence events not resolved at $1.2''$. Our current study does not provide conclusive evidence that such subscale events are the dominant source of new flux on the Sun, but it is consistent with that picture. We *are* able to conclude that most flux in the solar network has been processed by unresolved events such as shredding, coalescence, and bipolar emergence. We note that strong random, diverging flows are not currently observed on scales smaller than granules, and we surmise that any currently unresolved shredding is most likely to be due to interaction with emerging unresolved bipoles.

Schrijver et al. (1997) presented a measured exponential flux distribution function at moderate flux ranges and stated that it was indicative of a dynamic equilibrium between competing processes: the breakup of large flux concentrations and the coalescence of smaller flux concentrations. The observations are difficult at the large end of the flux distribution function due to the low number of events and are also difficult at the small end of the flux distribution function due to the small size of the flux concentrations. Since the small end of the distribution has been so poorly constrained, most models (such as those of Simon et al. 2001) have focused on the breakup of large concentrations to form the network. The present results suggest that proper modeling of network formation must include the coalescence of subarcsecond flux concentrations. By comparing concurrent quiet-Sun *Hinode* and MDI magnetograms, it should be possible to regularly observe the aggregation of intranetwork concentrations into larger flux concentrations.

The source term for the magnetochemistry equations is difficult to determine observationally, and Schrijver et al. (1997) considered two special cases: that all the flux is injected in the form of 10^{19} Mx ephemeral regions, and that all flux that is canceled in an opposite-polarity collision resurfaces some short time later. The latter was found to produce a distribution of fluxes that was incompatible with what is observed, and thus they concluded that the ephemeral region flux is not recycled flux, but bona fide new flux. The current work suggests the presence of a component of the source function that operates at the small end of the flux distribution, in addition to the ephemeral region component that operates at the large end of the distribution. Given the fact that the magnetochemistry equations concern the evolution of flux concentrations detected at a given resolution, at present this would require the addition of two terms: Gain by Appearance and Loss by Disappearance. These new terms would become unnecessary if the resolution of future solar magnetographs enables the observation of the fundamental flux production process.

D. A. L. and C. E. D. acknowledge support by a grant from the NASA SR&T-SHP program. B. T. W. acknowledges support via NSF grant ATM 0451438. We thank the referee for a clear review that aided in the improvement of the paper. We also thank the University of St. Andrews for hosting our first meeting, Lockheed Martin for hosting our second meeting, and to the *SOHO* MDI team for generously sharing their data. *SOHO* is a project of international collaboration between ESA and NASA.

REFERENCES

Berger, T. E., & Title, A. M. 2001, ApJ, 553, 449
Berger, T. E., et al. 2004, A&A, 428, 613
Cattaneo, F., Emonet, T., & Weiss, N. 2003, ApJ, 588, 1183
Choudhuri, A. R. 1992, A&A, 253, 277
DeForest, C. E. 2004, Sol. Phys., 219, 3
DeForest, C. E., Hagenaar, H. J., Lamb, D. A., Parnell, C. E., & Welsch, B. T. 2007, ApJ, 666, 576 (Paper I)
DeForest, C. E., & Lamb, D. A. 2004, BAAS, 36, 687
De Pontieu, B. 2002, ApJ, 569, 474
Freeland, S. L., & Handy, B. N. 1998, Sol. Phys., 182, 497
Hagenaar, H. J. 2001, ApJ, 555, 448
Hagenaar, H. J., Schrijver, C. J., & Title, A. M. 1997, ApJ, 481, 988
———. 2003, ApJ, 584, 1107
Hagenaar, H. J., Schrijver, C. J., Title, A. M., & Shine, R. A. 1999, ApJ, 511, 932
Hagenaar, H. J., & Shine, R. A. 2005, ApJ, 635, 659
Hart, A. B. 1954, MNRAS, 114, 17
Harvey, J. W., Branston, D., Henney, C. J., & Keller, C. U. 2007, ApJ, 659, L177
Harvey, K. L. 1993, Ph.D. thesis, Univ. Utrecht
Kosovichev, A., et al. 1997, Sol. Phys., 170, 43
Krijger, J. M., & Roudier, T. 2003, A&A, 403, 715
Leighton, R. B., Noyes, R. W., & Simon, G. W. 1962, ApJ, 135, 474
Lites, B. W., Leka, K. D., Skumanich, A., Martinez Pillet, V., & Shimizu, T. 1996, ApJ, 460, 1019
Martin, S. F. 1988, Sol. Phys., 117, 243
Scherrer, P. H., et al. 1995, Sol. Phys., 162, 129
Schrijver, C. J., Title, A. M., van Ballegooijen, A. A., Hagenaar, H. J., & Shine, R. A. 1997, ApJ, 487, 424
Simon, G. W., Title, A. M., & Weiss, N. O. 2001, ApJ, 561, 427